Structural studies of charge disproportionation and magnetic order in $CaFeO_3$

P. M. Woodward*
Department of Chemistry, The Ohio State University, Columbus, Ohio 43210-1185

D. E. Cox and E. Moshopoulou†
Department of Physics, Brookhaven National Laboratory, Upton, New York 11973

A. W. Sleight
Department of Chemistry and Center for Advanced Materials Research, Oregon State University, Corvallis, Oregon 97331

S. Morimoto
Graduate School of Engineering Science, Osaka University, Toyonaka 560-8531, Japan
(Received 21 December 1999)

The crystal and magnetic structures of $CaFeO_3$ have been determined at 300 and 15 K using synchrotron x-ray and neutron powder-diffraction techniques. At 300 K, $CaFeO_3$ adopts the $GdFeO_3$ struture, space group *Pbnm* with unit-cell dimensions $a=5.326\,30(4)$, $b=5.352\,70(4)$, and $c=7.539\,86(6)$ Å. This structure is distorted from the ideal perovskite structure by tilting of the FeO_6 octahedra about [110] and [001]. The average Fe-O distance is 1.922(2) Å, and the Fe-O-Fe angles are 158.4(2)° and 158.1(1)°. At 15 K the crystal structure belongs to space group $P2_1/n$ with $a=5.311\,82(3)$, $b=5.347\,75(4)$, $c=7.520\,58(5)$ Å and $\beta=90.065(1)°$, and contains two distinct Fe sites. The average Fe-O bond length is 1.872(6) Å about the one iron site, and 1.974(6) Å about the second site, with bond valence sums of 4.58 and 3.48, respectively. This provides quantitative evidence for charge disproportionation, $2Fe^{4+}\rightarrow Fe^{3+}+Fe^{5+}$, at low temperature. The temperature evolution of the lattice parameters indicates a second- (or higher-) order phase transition from the orthorhombic charge-delocalized state to the monoclinic charge-disproportionated state, beginning just below room temperature. The magnetic structure at 15 K is incommensurate, having a modulation vector $[\delta,0,\delta]$ with $\delta\sim0.322$, corresponding to one of the $\langle111\rangle$ directions in the pseudocubic cell. A reasonable fit to the magnetic intensities is obtained with the recently proposed screw spiral structure [S. Kawasaki *et al.*, J. Phys. Soc. Jpn. **67**, 1529 (1998)], with Fe moments of 3.5 and $2.5\mu_B$, respectively. However, a comparable fit is given by a sinusoidal amplitude-modulated model in which the Fe moments are directed along [010], which leaves open the possibility that the true magnetic structure may be intermediate between the spiral and sinusoidal models (a fan structure).

INTRODUCTION

The contrasting structural, magnetic, and electronic behavior of the high spin d^4 $(t_{2g}^3e_g^1)$ transition-metal perovskites $LaMnO_3$, $SrFeO_3$, and $CaFeO_3$ have long been of interest to condensed matter scientists. $LaMnO_3$ is an antiferromagnetic (*A*-type) insulator, which exhibits a pronounced cooperative Jahn-Teller distortion of the MnO_6 octahedra.[1,2] Both the magnetic structure and the Jahn-Teller distortion are consistent with the presence of localized electrons and a homogeneous distribution of Mn^{3+} ions. In $SrFeO_3$ strong covalency in the Fe:e_g-O:$2p\sigma$ interaction leads to formation of a σ^* band and electron delocalization.[3] This change in the electronic band structure, with respect to $LaMnO_3$, is evident in the electronic transport properties (metallic down to at least 4.2 K) and crystal structure (undistorted cubic perovskite) of $SrFeO_3$.[4–7] Delocalization of the e_g electrons also occurs in $CaFeO_3$ at room temperature giving rise to metallic conductivity. However, transport measurements show a metal-insulator transition near 290 K.[7] Mössbauer effect (ME) studies of $CaFeO_3$ at 4.2 K reveal the presence of two chemically distinct iron sites with different hyperfine fields present in equal proportions.[8] This observation has led to the widely held view that charge disproportionation of the type, $2Fe^{4+}$ $(d^4)\rightarrow Fe^{3+}$ $(d^5)+Fe^{5+}$ (d^3), occurs in $CaFeO_3$. However, a study of the hyperfine parameters as a function of temperature has shown that this charge disproportionation occurs in varying degrees, corresponding to the charge states $Fe^{(4-\delta)+}$ and $Fe^{(4+\delta)+}$.[9] Furthermore, recent x-ray and UV photoemission measurements have demonstrated that the $(FeO_6)^{8-}$ octant is characterized by a large negative effective charge-transfer energy, such that the Fe(IV) and Fe(V) oxidation states can be approximated as Fe^{+3} ions accompanied by single or double oxygen holes $d^5\underline{L}$ and $d^5\underline{L}^2$, respectively.[10] In this view, the charge disproportionation may thus be rewritten as $2d^5\underline{L}\rightarrow d^5+d^5\underline{L}^2$. Regardless of the nomenclature one chooses it is very clear that when iron is in an elevated oxidation state [Fe(IV), Fe(V), or Fe(VI) (Ref. 11)] its interaction with oxygen is highly covalent. Throughout this paper we will use the former notation, $2Fe^{4+}\rightarrow Fe^{3+}+Fe^{5+}$, but it should be understood that we are referring to oxidation states rather than real charges.[12] Both $SrFeO_3$ and $CaFeO_3$ are reported to possess a spiral antiferromagnetic spin structure, with Néel temperatures of 134 and 115 K, respectively.[6,7,13,14] Thus each compound removes the orbital degeneracy of the $t_{2g}^3e_g^1$ configu-

ration in a different way: $LaMnO_3$ through a cooperative Jahn-Teller distortion, $SrFeO_3$ through band formation/electron delocalization, and $CaFeO_3$ through a charge disproportionation.

Stoichiometric $CaFeO_3$ was prepared almost 30 years ago by Kanamaru *et al.*,[15] who reported the crystal structure to be cubic. Subsequent studies by Takeda *et al.* reported a slight tetragonal distortion of the structure.[13] More recently, Morimoto *et al.* reported the room-temperature structure to be orthorhombic, space group *Pbnm*, and the low-temperature structure to be monoclinic, space group $P2_1/n$.[16] These space-group assignments imply that the room-temperature structure is distorted from the ideal cubic perovskite structure by the same octahedral tilting distortion seen in $GdFeO_3$ and $CaTiO_3$, while the low-temperature charge disproportionation introduces a rock salt ordering of Fe^{3+} and Fe^{5+}. However, detailed structural information to support these conclusions was not provided. In fact, despite the relatively large body of work devoted to charge disproportionation in $CaFeO_3$ over the past 29 years, there is still a complete lack of detailed structural information for this compound in either the charge-delocalized or charge-disproportionated states. This is somewhat surprising in light of the fact that such information is of critical importance in order to fully understand this relatively rare and intriguing metal-insulator phase transition. If the Fe in $CaFeO_3$ disproportionates at low temperature, there should be evidence of this from diffraction. This prompted us to undertake a structural study of $CaFeO_3$ using synchrotron x-ray and neutron powder-diffraction techniques.

EXPERIMENT

Synthesis of a polycrystalline $CaFeO_3$ sample was performed under high oxygen pressure. $CaFeO_{2.5}$ was used as starting material and $KClO_4$ as an oxygen source. These compounds were sealed into a gold capsule and separated by ZrO_2. The capsule was then annealed at 1227 under 3 GPa for 1 h, according to the procedure described in Ref. 13. X-ray diffraction showed the sample to contain a very small amount of an unidentified impurity phase (see Fig. 1), but otherwise the peak shapes were sharp and symmetric indicative of a compositionally homogeneous sample. Analysis of the neutron-diffraction data gave no indication of oxygen vacancies.

X-ray powder-diffraction data were collected on beamline X7A of the National Synchrotron Light Source, located at Brookhaven National Laboratory. Data were collected several times in one of two instrumental configurations. High-resolution variable-temperature measurements were taken by mounting a portion of the sample onto a flat-plate Cu sample holder and loading it into a closed-cycle helium cryostat in symmetric reflection geometry. To obtain optimal resolution a double-crystal Ge(111) monochromator was used in the incident beam, and a flat Ge(220) analyzer crystal (CA) in the diffracted beam. This configuration not only gives very high resolution [instrumental broadening, full width at half maximum (FWHM) $\sim 0.01°$ at $\lambda = 1.2$ Å], but also greatly reduces background noise, including scattering from the beryllium windows of the cryostat. Finally, to improve powder averaging the sample was rocked over a few degrees at each step. The wavelengths and counting times employed for each measurement are given in the results section.

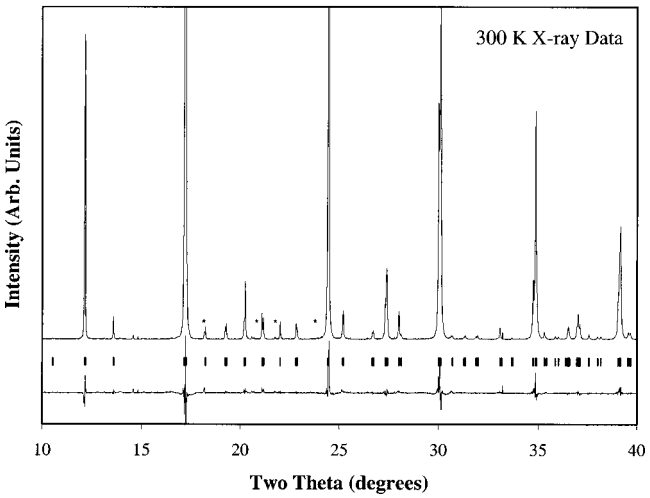

FIG. 1. An expanded region of the observed x-ray-diffraction pattern of $CaFeO_3$ at 300 K (upper curve), and the difference curve I_{obs}-I_{calc} (lower curve). Tick marks denote the expected peak positions. The calculated diffraction pattern is omitted for clarity. The peaks marked with an asterisk arise from the presence an minute amount of an unknown impurity phase.

Additional x-ray data were collected at a wavelength of 0.6949 Å with a linear position-sensitive detector (PSD) mounted on the scattering arm in place of the crystal analyzer. The linear PSD is a proportional multiwire device of the type described by Smith.[17] For these measurements, the sample was loaded into a 0.2-mm-diameter thin-walled glass capillary and mounted in the cryostat. In this configuration, the instrumental resolution is somewhat lower (FWHM $\sim 0.03°$ at $\lambda = 1.2$ Å) but the counting rates are much faster, enabling extended scans to be made with good counting statistics in a few hours. Furthermore, the use of capillary geometry and larger rocking angles reduces systematic errors due to preferred orientation and inadequate powder averaging. Consequently, the data sets generally yield Rietveld fits of excellent quality. This instrumental configuration ($\lambda = 0.6941$ Å) was employed while collecting the data which were subsequently used to determine the temperature evolution of the unit-cell parameters, as well as an extended data set used in the refinement of the low-temperature structure.

Finally, constant wavelength neutron powder-diffraction data were collected at the NIST reactor at 300 and 15 K at a wavelength of 2.078 Å on the high-resolution powder diffractometer BT1, which is equipped with a bank of 32 detectors and horizontal collimators with a divergence of $7'$. Because of the relatively small sample size (~ 0.35 g), the in-pile collimation was relaxed to $14'$. The detector bank was stepped at 0.05° intervals. Structure refinements were performed using the Rietveld method as implemented in the GSAS software suite,[18] while the magnetic structure was refined using the FULLPROF program.[19] In order to obtain the most accurate crystal structure results, two data sets were refined simultaneously at both 300-K (x-ray CA and neutron data) and 15-K (x-ray PSD and CA data). One problem inherent to combined refinements of multiple data sets is that systematic errors in data collection can lead to slight differences in the lattice parameters and displacement parameters

TABLE I. Results of Rietveld refinements at 300 and 15 K.

Radiation	Neutron	X ray (CA)	X ray (PSD)	X ray (CA)
Temperature (K)	298		15	
R_{wp}	6.37%	9.77%	4.51%	18.46%
R_p	5.00%	6.62%	2.89%	12.04%
$R(F^2)$	6.38%	3.91%	5.53%	6.92%
χ^2	2.39		9.82	
Wavelength	2.080	0.7992	0.6949	1.1918
2θ range (°)	5–150	9–55	9–71	10–42
No. of reflections	104	200	1043	52
No. of variables	28		35	
Space group	*Pbnm*		$P2_1/n$	
a (Å)	5.326 31(4)		5.311 82(3)	
b (Å)	5.352 81(4)		5.347 75(4)	
c (Å)	7.539 87(5)		7.520 58(5)	
β (°)	90		90.065(1)	
Volume (Å^3)	214.967(3)		213.632(4)	

determined for each data set. To avoid this complication, the wavelength of the x-ray data set collected with the CA detector was fixed, while the wavelength of the second data set was refined. Despite the introduction of an additional variable the refined wavelength values were found to be very close to their expected values for both the 300 K neutron data set (refined $\lambda = 2.080$ Å, expected $\lambda = 2.077$ Å) and the 15 K x-ray PSD data set (refined $\lambda = 0.6949$ Å, expected $\lambda = 0.6941$ Å). To account for differences in displacement parameters, an absorption correction for surface roughness (according to Suorti)[20] was applied to the x-ray data collected on the flat plate sample with the CA detector. Once these two corrections were applied we found that the goodness of fit indicators from the combined refinements were very similar to those obtained from refining data sets independently.

RESULTS AND DISCUSSION

Room-temperature structure determination

The beginning point of our study was determination of the $CaFeO_3$ crystal structure above the charge-disproportionation (CD) temperature $T_{CD} \sim 290$ K. Two high-resolution data sets were collected at room temperature: a synchrotron x-ray-diffraction pattern collected in the CA configuration, and a neutron-diffraction pattern. Each data set was refined independently and in a combined refinement, where both x-ray and neutron patterns were simultaneously refined using a single structural model. There was very good agreement between the results of the independent refinements and the combined refinement. The results of the combined refinement are listed in Tables I and II, while the bond distances, angles, and valences are listed in Table III. Fits to the experimental diffraction patterns are shown in Figs. 1 and 2.

The results confirm earlier reports by Morimoto *et al.* that $CaFeO_3$ is isostructural with $GdFeO_3$ and $CaTiO_3$ at room temperature.[16] Distortions of the FeO_6 octahedra are very small, and the Fe-O distances are very similar to the ~1.925-Å distance observed in $SrFeO_3$ at room temperature.[6] In fact, the bond valences for all ions (see Table III) are very near their ideal values, suggesting a stable, accurately determined structure. The octahedral tilting distortion results in a significant bending of the Fe-O-Fe bonds away from the linear 180° value observed in $SrFeO_3$. This reduces the spatial overlap of the Fe e_g orbitals with the O $2p\sigma$ orbitals, which in turn reduces the σ^* bandwidth, and is largely responsible for the contrasting behavior of $CaFeO_3$ and $SrFeO_3$. Finally, we note that the results of refinements based on neutron and x-ray data are in excellent agreement. Since neutron-diffraction measurements normally give more accurate structures for metal oxides, this agreement clearly demonstrates the accuracy of the synchrotron x-ray data.

Confirmation of charge disproportionation

There have been many crystallographic studies of cation ordering in perovskites. For compounds containing two octahedral cations in equal proportions, $A_2MM'X_6$, the most favorable arrangement of these cations is invariably a rock-salt-type ordering of the M and M' ions. This leads to a structure where each MX_6 octahedron is surrounded by six $M'X_6$ octahedra and vice versa. This arrangement not only optimizes the Coulomb interactions within the crystal, but can accommodate a cooperative distortion of the oxygen network without introducing strain into the M-X and M'-X bonds. In $CaFeO_3$ such a distortion can be described as the freezing out of a phonon breathing mode. The relatively few cases where an alternate cation ordering arrangement is observed for an $A_2MM'X_6$ compound, such as

TABLE II. Fractional coordinates and displacement parameters for $CaFeO_3$ at 300 K.

Atom	Site	x	y	z	B(iso)
Ca	4c	0.9950(3)	0.0328(1)	0.25	1.22(2)
Fe	4b	0	0.5	0	0.92(1)
O1	8d	0.7129(4)	0.2858(3)	0.0327(3)	1.05(6)
O2	4c	0.0663(6)	0.4908(4)	0.25	1.29(4)

TABLE III. Bond distances, bond angles, and bond valences for $CaFeO_3$ at 300 K.

Bond distances (Å)	
Fe-O1	2×1.920(2)
	2×1.927(2)
Fe-O2	2×1.9184(6)
Fe-O (avg)	1.922(2)
Bond angles (°)	
O1-Fe-O1	2×89.37(2)
	2×90.63(2)
O1-Fe-O2	2×89.8(1)
	2×89.7(1)
	2×90.3(1)
	2×90.2(1)
Fe-O1-Fe	157.9(1)
Fe-O2-Fe	158.6(2)
Bond valences[a]	
Ca	2.19
Fe	3.71 (4.01)
O1	1.95 (2.05)
O2	1.99 (2.09)

[a]Bond valences were calculated using the program VALENCE (Ref. 45). The default ρ_0 values were used (1.967 for the Ca-O interaction and 1.744 for the Fe^{4+}-O interaction). Values in parentheses were calculated using $\rho_0 = 1.772$ for Fe^{4+}-O. This value of ρ_0 was obtained by assuming the ideal six coordinate Fe^{4+}-O distance was 1.922 Å.

$LaCaMn^{3+}Mn^{4+}O_6$,[21] $NdSrMn^{3+}Mn^{4+}O_6$,[22] and La_2CuSnO_6,[23] all contain octahedra which are distorted due to the presence of a Jahn-Teller cation. Therefore we started with the premise that the low-temperature structure should contain a 1:1 rock salt ordering of Fe^{3+} and Fe^{5+}.

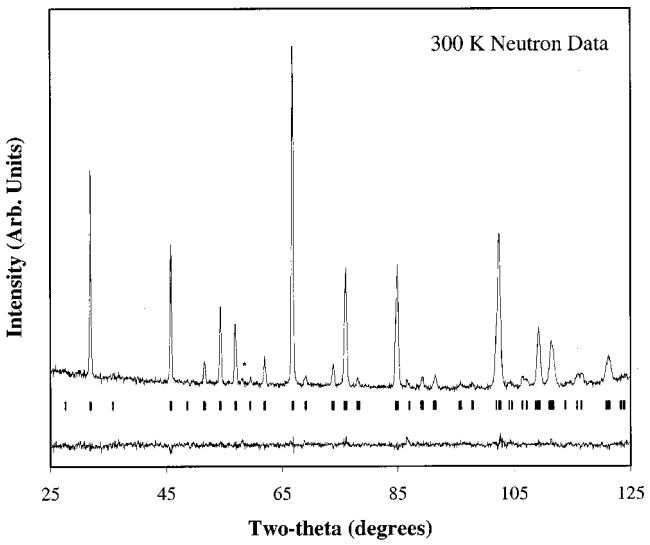

FIG. 2. A portion of the observed neutron-diffraction pattern of $CaFeO_3$ at 300 K (upper curve), and the difference curve I_{obs}-I_{calc} (lower curve). Tick marks denote the expected peak positions. The calculated diffraction pattern is omitted for clarity. The peaks marked with an asterisk arise from the presence an minute amount of an unknown impurity phase.

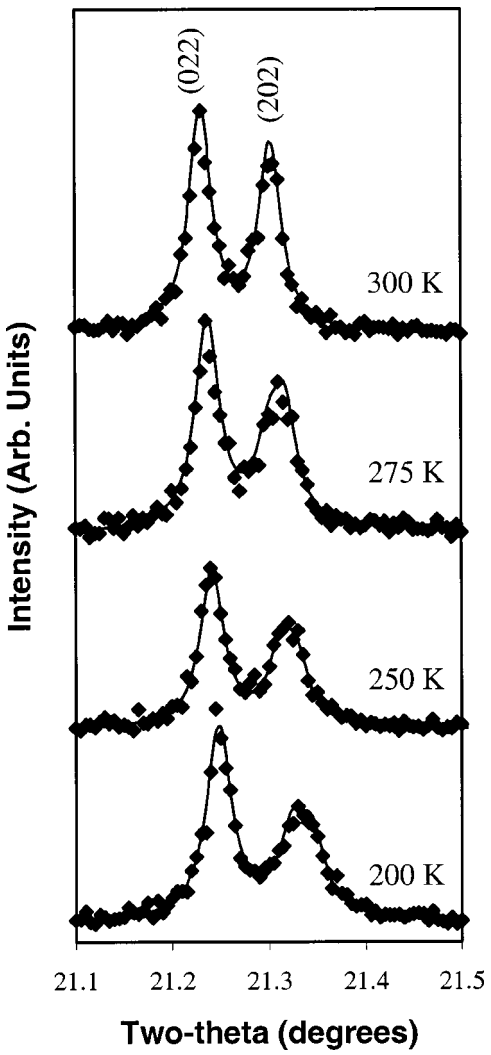

FIG. 3. The (022) and (202) peaks in the x-ray-diffraction pattern (CA detector, $\lambda = 0.8038$ Å, step size = 0.005°, count rate = 8 sec/step) at various temperatures. The solid lines represent peak fitting results using a Lorentzian peak shape and a single FWHM for all peaks. The 300-K data are fit with two peaks, the (022) and the (202), while the other data sets are fit with three peaks, the (022), $(\bar{2}02)$, and (202) reflections.

The combination of in-phase tilting of the octahedra about [001], out-of-phase tilting of the octahedra about [110] (Glazer tilt system $a^-a^-b^+$),[24] and 1:1 rock salt cation ordering is known to produce a monoclinic structure with $P2_1/n$ symmetry and approximate unit-cell dimensions: $a \approx \sqrt{2}a_p$, $b \approx \sqrt{2}a_p$, $c \approx 2a_p$, and $\beta \approx 90°$ (where a_p is the simple perovskite cell edge, $a_p \approx 3.9$ Å).[25] Anderson *et al.*[26] have shown that for perovskites, distorted by $a^-a^-b^+$ octahedral tilting, the presence of $0kl: k = 2n+1$ reflections is evidence for an ordered arrangement of octahedral cations. Furthermore, the reduction in symmetry from orthorhombic to monoclinic should be evident in a slight deviation of β from 90°.[27]

Figure 3 shows the orthorhombic (022) and (202) reflections at 300, 275, 250, and 200 K. If β deviates from 90° the (202) reflection will be split into two peaks of equal intensity, $(\bar{2}02)$ and (202), while the (022) peak will be unaffected. Although the distortion is not large enough to split

the latter peak into two distinct peaks, the width of the (202) reflection is clearly increasing as the temperature decreases, consistent with the presence of a slight monoclinic distortion. Both lattice parameter refinements based on individually determined peak positions (using the peak fitting routine in the CMPR software package)[28] and the whole pattern fitting employed in the Rietveld refinement technique, indicate a slight monoclinic distortion at 275 K and an unmistakable monoclinic distortion at 250 K.

Our observation that a monoclinic distortion of the unit cell occurs below the metal-insulator transition lends support to the claims of CD in $CaFeO_3$. The appearance of one or more $0kl:k=2n+1$ reflections would confirm the presence of a long-range cooperative CD. Due to the fact that only the oxygen ions are expected to be significantly displaced as a consequence of the CD, we expect any extra peaks in the x-ray-diffraction pattern to be very weak. In order to guide our search for such peaks a model CD low-temperature structure was generated using the software package POTATO.[29] The octahedral tilt angles were derived from the room-temperature structure as was the position of the Ca^{2+} ion. The Fe^{3+}-O and Fe^{5+}-O distances were taken to be 1.985 and 1.865 Å, respectively. The program Lazy-Pulverix[30] was then used to calculate the expected peak intensities for the CD structure and a structure where all of the Fe-O distances remain equivalent. The results are listed in Table IV. This calculation shows that the ''extra peaks'' which arise due to the charge disproportionation are very weak; the strongest such peak is the (011), whose intensity is 500 times smaller than the strongest reflection. The sensitivity and excellent peak-to-background discrimination of the X7A powder diffractometer, should be sufficient to detect the (011) reflection given sufficient counting times. However, calculated intensities of the other ''CD peaks'' are so small, that it is unlikely one would be able to distinguish them from background noise.

Figure 4 shows the region of the diffraction pattern, where the (011) and (101) reflections are expected, at three different temperatures: 300, 200, and 15 K. The presence of the (011) reflection is clearly seen at 200 and 15 K, but is absent at 300 K. To obtain the data shown in Fig. 4 it was necessary to use the crystal analyzer detector in order clearly resolve the (011) and (101) reflections and to minimize the noise from the beryllium windows of the cryostat. In order to obtain the excellent statistics needed to confirm the presence of such weak peaks a step size of 0.005° and counting time of 240 sec per step were used. Taken together with our observation of a monoclinic distortion, this confirms the presence of a CD corresponding to a rock salt ordering of Fe^{3+} and Fe^{5+} below the metal-insulator transition at 290 K.

Low-temperature structure determination

Having confirmed CD in $CaFeO_3$, the next step is to determine the low-temperature structure. Since the structural transformation which is expected to accompany the CD phase transition involves primarily displacements of oxygen ions, neutron diffraction would seem to be the logical tool for determining the low-temperature structure. However, at low temperatures where the CD has fully set in, the neutron-diffraction pattern is complicated by magnetic reflections arising due to the presence of an incomensurate antiferromagnetic spin structure, which will be discussed in more detail in the following section. An alternative approach is to refine the structure from x-ray-diffraction data. At first glance it may seem unlikely that a stable refinement could be obtained from an x-ray-diffraction pattern with essentially one superlattice peak. However, Table IV shows that the intensities of several of the weaker reflections are quite sensitive to the CD distortion. These peaks owe their existence to both octahedral tilting and CD (cation ordering) distortions. This observation, coupled with the accuracy of the room-temperature x-ray refinements, suggests that it may be possible to obtain an accurate structure refinement from high-quality x-ray-diffraction data.

TABLE IV. Calculated X-ray diffraction peak intensities in the presence and absence of CD.

hkl	Relative intensity $CaFe^{4+}O_3$ model	Relative intensity $Ca_2Fe^{3+}Fe^{5+}O_6$ Model[c]
011[a]		**1.7**
101	*0.3*	*2.0*
110	140	140
002	65.6	65.7
111	16.3	16.3
012[a]		**0**
020	254	254
112	1000	1000
200	235	235
021	8.4	8.3
120	8.2	9.2
210	11.3	12.5
121[b]	*14.6*	*19.6*
013[a]		**0.2**
211[b]	*22.7*	*15.6*
103[b]	*31.2*	*36.3*
022	31.9	31.3
202	25.4	24.9
113	13.9	13.8
122	11.3	9.8
212	9.4	7.9
220	479	475
004	251	249

[a]Reflections marked in bold represent peaks which are not allowed in the absence of CD.

[b]Reflections marked in italics represent peaks whose intensities are sensitive the CD distortion.

[c]Details of the structure model employed are given in the text. For the monoclinic phase *hkl* and $\bar{h}kl$ peak intensities have been combined to give the intensity of the *hkl* peak.

Two sets of x-ray-diffraction data were collected at 15 K and refined simultaneously using the GSAS software suite. The first data set was collected in the CA mode ($\lambda = 1.1918$ Å, step size$=0.005°$). Very long counting times (240 sec) were used over narrow regions containing potential superstructure reflections in order to obtain optimal statistics. However, it is not feasible to collect the entire data set using these parameters (a scan from 10–50° would take over 22

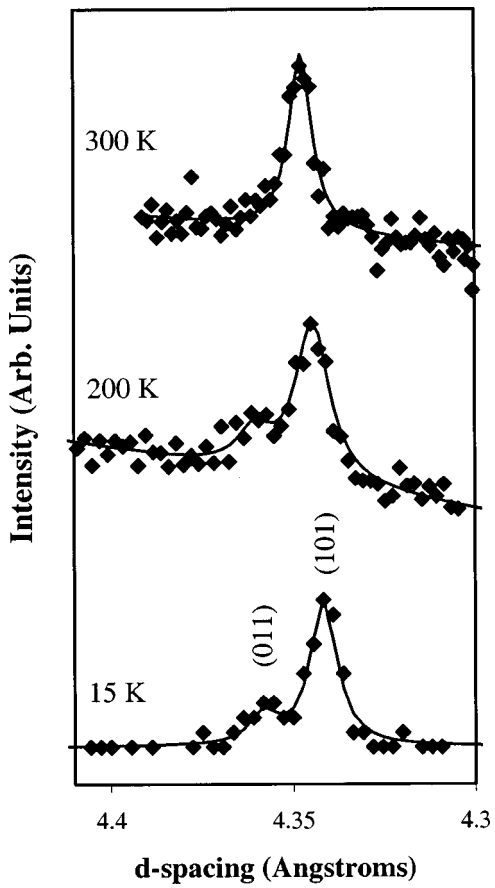

FIG. 4. The region of the x-ray-diffraction pattern containing the (011) and (101) reflections. Solid lines represent peak fitting results using a Lorentzian peak shape and a single FWHM for both peaks (one peak in the 300 K data).

days at that rate), so counting times varying from 4 to 16 sec per step were used over the rest of the pattern. The high resolution and minimal background obtained using this instrumental configuration are well suited for the high degree of pseudosymmetry and weak superstructure reflections associated with the CD structure. Unfortunately, the slow rate of data collection, and time constraints inherent to experiments conducted at a synchrotron source, only allowed data collection over a limited angular range ($2\theta = 10-42°$, $d_{\min} = 1.66$ Å, 52 reflections). To compensate for this a second data set was collected at a wavelength of 0.6949 Å, using the linear PSD detector. This instrumental configuration provided a data set with good statistics over an extended angular range ($2\theta = 9-71°$, $d_{\min} = 0.60$ Å, 1043 reflections), with a small decrease in the resolution and the introduction of some noise in the low angle region (due to reflection from the Be windows of the cryostat). The refinement results are given in Tables I and V, while the bond distances, angles, and valences are contained in Table VI. The refined fit to the PSD data set is shown in Fig. 5, and a polyhedral representation of the structure is shown in Fig. 6.

Comparison of the crystal structures determined at 300 and 15 K shows that the structural change which accompanies the charge disproportionation involves condensation of a breathing phonon mode leading to a rock salt ordering of Fe^{3+} and Fe^{5+}, as had been previously proposed.[31] The Fe-O distances clearly show two chemically distinct iron sites. No change in the octahedral tilt system is observed, although the Fe-O-Fe angles appear to decrease slightly. The bond valences of the calcium and oxygen ions are close to their expected values, providing further confirmation of the accuracy of the structure determination. The octahedral distortions increases with respect to the room-temperature structure, most likely as a result of strains in the Ca-O bonding network and the reduction in symmetry. The bond valence sums of 4.58 (Fe1) and 3.48 (Fe2) clearly indicate the differing chemical environments of the two sites, but do not reach the ideal values expected for a full disproportionation into Fe^{5+} and Fe^{3+}. However, it should be noted that bond

TABLE V. Fractional coordinates and displacement parameters for $CaFeO_3$ at 15 K.

Atom	Site	x	y	z	B(iso)[a]
Ca	4e	0.9936(4)	0.0371(1)	0.2511(6)	0.30(1)
Fe1	2d	0.5	0	0	0.308(8)
Fe2	2c	0	0.5	0	0.308(8)
O1	4e	0.300(1)	0.720(1)	−0.0330(7)	0.43(4)
O2	4e	0.219(1)	0.206(1)	−0.0318(7)	0.43(4)
O3	4e	0.0761(6)	0.4927(5)	0.254(1)	1.10(6)

[a]The Fe1 and Fe2 displacement parameters were constrained to be equal, as were the O1 and O2 displacement parameters.

TABLE VI. Bond distances, bond angles, and bond valences for $CaFeO_3$ at 15 K.

Bond distances (Å)	
Fe1-O1	1.853(5)
Fe1-O2	1.870(5)
Fe1-O3	1.894(8)
Fe1-O (avg)	1.872(6)
Fe2-O1	1.997(5)
Fe2-O2	1.971(5)
Fe2-O3	1.953(9)
Fe2-O (avg)	1.974(6)
Bond angles (°)	
O1-Fe1-O2	89.9(4)/90.1(4)
O1-Fe1-O3	89.5(2)/90.5(2)
O2-Fe1-O3	88.0(2)/92.0(2)
O1-Fe2-O2	89.0(4)/91.0(4)
O1-Fe2-O3	88.2(2)/91.8(2)
O2-Fe2-O3	88.9(2)/91.1(2)
Fe2-O1-Fe1	156.5(3)
Fe2-O2-Fe1	157.8(8)
Fe2-O3-Fe1	155.6(2)
Bond valences[a]	
Ca	2.27
Fe1	4.58
Fe2	3.48
O1	2.10
O2	2.08
O3	2.12

[a]Bond valences were calculated using the program VALENCE (Ref. 45). The valences of the Fe-O bonds were calculated using the ρ_0 value (1.772) determined at 300 K for Fe^{4+}.

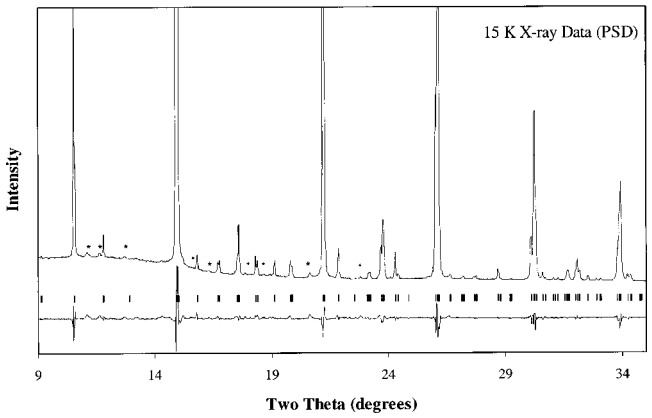

FIG. 5. An expanded region of the observed x-ray-diffraction pattern of $CaFeO_3$ at 15 K (upper curve), and the difference curve I_{obs}-I_{calc} (lower curve). Tick marks denote the expected peak positions. The calculated diffraction pattern is omitted for clarity. The peaks marked with an asterisk arise from the presence of a minute amount of an unknown impurity phase, as well as from scattering from the Be windows of the cryostat (the three peaks between 10 and 13° 2θ and the peak at ~22° 2θ).

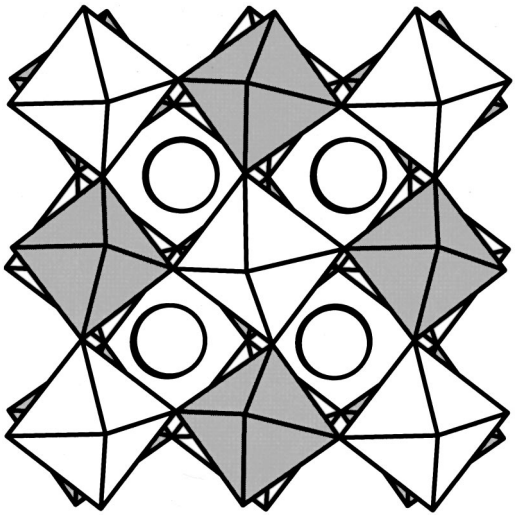

FIG. 6. A polyhedral representation of the crystal structure of $CaFeO_3$ at 15 K. Fe2 resides at the center of the unshaded octahedra, while Fe1 is found at the center of the shaded octahedra. The open spheres represent calcium ions.

valence calculations do not indicate a full charge disproportionation in a variety of other compounds that undergo similar transitions (see Table VII). The degree of CD in $CaFeO_3$, as calculated from bond valence calculations, is intermediate between $YNiO_3$, where the CD occurs at a higher temperature and has a much stronger influence on the lattice,[32] and $BaBiO_3$ where the CD is strong enough to exist up to ~860 °C.[33] Furthermore, the isomer shift observed for $CaFeO_3$ in variable temperature Mössbauer spectra, which is very sensitive to the CD, remains essentially constant below about 160 K.[34] Fractional charges on ions are unphysical; likewise, fractional charges of oxidation states, which count electrons in the bonds rather than on the atoms, are not allowed at the atomic level. However, we may consider that in $CaFeO_3$ the ground state is the oxidation states Fe^{3+} and Fe^{5+} but that the nondisproportionated Fe^{4+} state is a low-lying excited state. Thus with increasing temperature this state becomes increasing populated until finally the disproportionated state is completely destroyed.

In order to investigate the nature of the CD phase transition, we determined the unit-cell parameters over the temperature range 100–315 K, in 15-K intervals. These values were obtained from Rietveld refinements of x-ray-diffraction data, collected using the PSD. The results are shown in Figs. 7–9. No sudden discontinuities were observed over this temperature range, consistent with a second- (or higher-) order CD phase transition. Finally, we note that the temperature evolution of β, which is one indicator of the degree of CD, is in qualitatively good agreement with the temperature evolution of the isomer shift $\Delta\delta$.[34]

Low-temperature magnetic structure

The low angle regions of the neutron patterns at 298 and 15 K are shown in Fig. 10. The 15-K pattern is characterized

TABLE VII. Bond valence sums[a] of perovskite compounds, which undergo charge disproportionation or charge ordering.

Compound	Data coll. temp. (K)	Transition temp. (K)	Bond valence $M^{n+\delta}$	Bond valence $M^{n-\delta}$	% CD[b]	Ref.
$Ca_2Fe^{V}Fe^{III}O_6$	15	290	4.58	3.48	55 %	
$NdSrMn^{IV}Mn^{III}O^6$	50	155	3.98	3.49	49 %	22
$Ba_2Bi^{V}Bi^{III}O_6$	300	~860	4.87	3.36	76 %	46
$Ba_2Bi^{V}Bi^{III}O_6$	300	~860	4.97	3.26	86 %	33
$Y_2Ni^{IV}Ni^{II}O_6$	300	580	2.76	2.28	24 %	32
$YBaCo^{III}Co^{II}O_5$	25	220	2.65	2.05	60 %	47

[a]Bond valence sums were calculated from the literature bond distances using the program VALENCE (Ref. 45) with the exception of $BaBiO_3$ where the bond valence parameters determined by McGuire and O'Keeffe were used (Ref. 48).

[b]The % charge disproportionation was calculated using the formula $100\times(V1-V2)/(O1\text{-}O2)$, where $V1$ and $V2$ are the bond valences of the metal ions, while O1 and O2 are the oxidation states of the same cations in a fully disproportionated state.

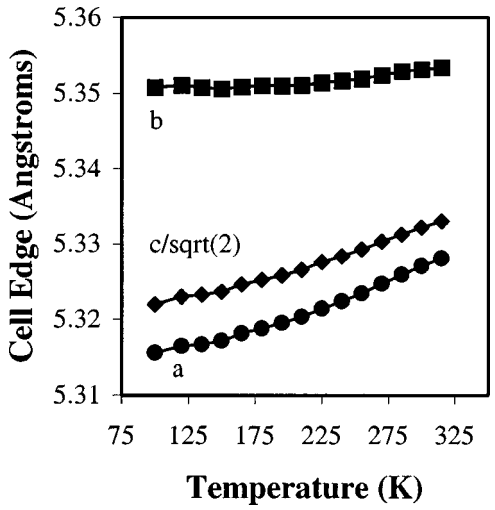

FIG. 7. The temperature evolution of the unit cell parameters a (circles), b (squares), and $c/\sqrt{2}$ (diamonds). Error bars are smaller than the symbols used to mark the points.

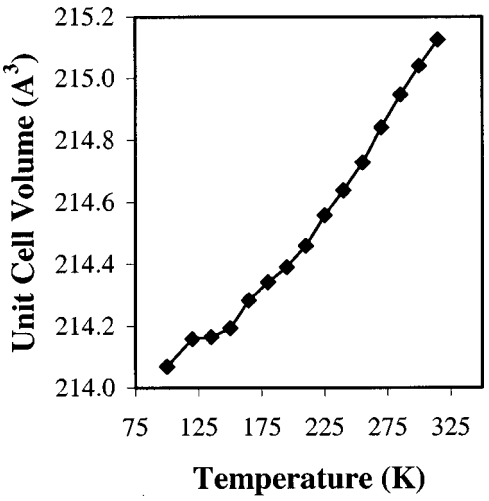

FIG. 9. The temperature evolution of the unit-cell volume. Error bars are smaller than the symbols used to mark the points.

by the appearance of additional peaks which are clearly magnetic in origin. Fits of the individual peaks to a pseudo-Voigt function show that the magnetic peaks are significantly broader than the nuclear ones and also that, with the exception of the strong peak at ~8.9°, they are split into at least two components. Furthermore, they cannot be indexed on the basis of the chemical cell nor any simple enlarged cell. However, the peak positions can be accounted for satisfactorily with an incommensurate pseudocubic propagation vector $[\delta,\delta,\delta]$ with $\delta=0.161$, in good agreement with the value recently reported by Kawasaki *et al.*[7] The first four magnetic peaks can then be indexed as various combinations of satellites of the pseudocubic (000), (100), (110), and (111) reflections, as indicated in Fig. 10, and the intensities are qualitatively consistent with those expected from the simple ferromagnetic spiral structure proposed by Kawasaki *et al.*

A precise determination of the magnetic structure is complicated for a variety of reasons; there are only a few well-resolved magnetic peaks, these peaks are significantly broadened, the low-temperature crystal structure is monoclinic, and finally δ is very close to $\frac{1}{6}$, so that satellites originating

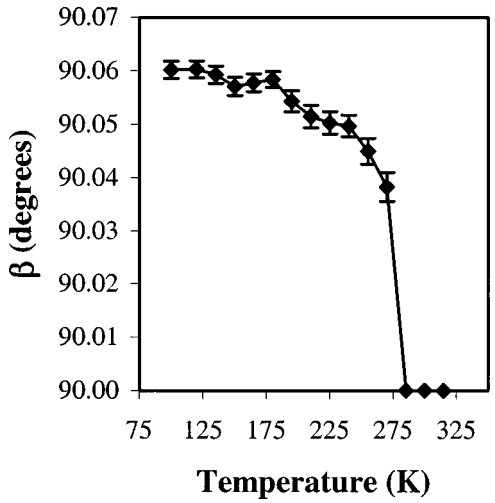

FIG. 8. The temperature evolution of the monoclinic angle β.

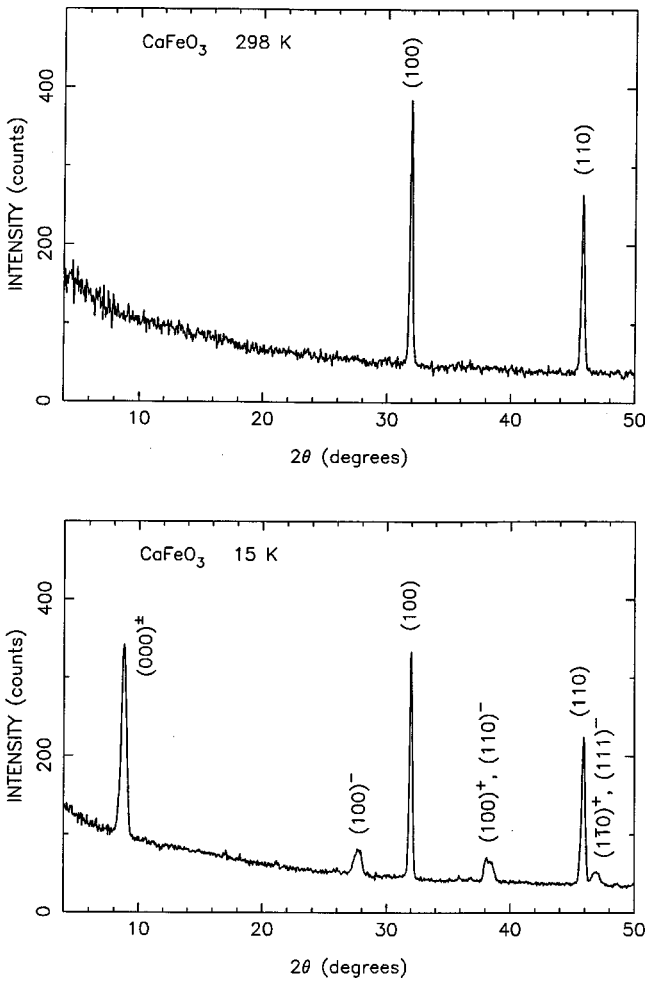

FIG. 10. Low angle region of the neutron patterns for $CaFeO_3$ at 298 K (upper) and 15 K (lower), with the peaks indexed on the basis of the pseudocubic unit cell. The $\pm$ superscripts on the indices of the magnetic peaks in the lower pattern signify ($h\pm\delta$, $k\pm\delta$, $l\pm\delta$).

TABLE VIII. Magnetic structure parameters for $CaFeO_3$ at 15 K for the constrained and unconstrained spiral and sinusoidal models described in the text. δ_a, δ_b, and δ_c are the components of the propagation vector in monoclinic reciprocal-lattice units. θ and φ are spherical angles defining the orientation with respect to the monoclinic [010] and [100] axes of either (a) the helical axis (spiral models 1A and 1B), or (b) the direction of the magnetic moments (sinusoidal models 2A and 2B). In the latter case, the ''moments'' represent the maximum amplitude of the sinusoidal modulation.

	Spiral		Sinusoidal	
	1A	1B	2A	2B
Fe1 moment (μ_B)	2.48(10)	2.70(13)	3.40(13)	3.60(14)
Fe2 moment (μ_B)	3.47(11)	3.52(13)	5.02(13)	5.06(14)
δ_a (Å^{-1})	0.3231(2)	0.3245(8)	0.3229(2)	0.3266(4)
δ_b (Å^{-1})	0.0	0.0095(8)	0.0	0.0
δ_c (Å^{-1})	0.3231	0.3191(12)	0.3229	0.3158(6)
θ (°)	90.0	71.4(1.4)	0.0	28.3(2.6)
φ (°)	35.2	56.2(9)	90.0	90.0
$R_{\rm nuc}$ (%)	2.9	2.8	2.9	2.9
$R_{\rm mag}$ (%)	7.2	4.5	7.5	5.8
$R_{\rm wp}$ (%)	3.9	3.8	3.9	3.9
χ^2	1.74	1.66	1.72	1.68

from different fundamental peaks are closely overlapped. Rietveld analysis was carried out with the FULLPROF program,[19] which allows incommensurate magnetic structures to be refined. If the cubic cell is transformed to the monoclinic cell via the matrix $[110;1\bar{1}0;002]$, the $\langle\delta\delta\delta\rangle$ propagation vectors become $\pm[\delta_m,0,\delta_m]$, $\pm[\delta_m,0,-\delta_m]$, and $\pm[0,\delta_m,\pm\delta_m]$, where $\delta_m=2\delta$. In general, the δ_m components of these propagation vectors are not required to be equal, nor need the other components be zero. In the following discussion, the directions and planes will be based on the monoclinic cell, but we shall sometimes specify the equivalent pseudocubic directions for clarity. In the initial stages, the magnetic peaks were excluded and the crystal structure and profile parameters were refined. The magnetic peaks were then included and the profile parameters refined from a LeBail fit[35] to the pattern with the crystal structure fixed and the two components of the propagation vector constrained to be equal. It was found that the broadening of the magnetic peaks could be accounted for very well by an additional particle-size parameter attributable to the formation of magnetic domains about 300 Å in size within the individual crystallites.

In addition to a simple helical structure, a sinusoidal amplitude-modulated model was also considered, since there is no *a priori* reason to rule out such structures. Antiphase-domain and helical-fan-type structures were not considered because of the absence of any satellite peaks associated with higher harmonics of the modulation vector. A series of refinements was first carried out for a simple ferromagnetic helix in which the helical axis (normal to the spiral plane) was fixed along the principal pseudocubic directions $\langle100\rangle$, $\langle110\rangle$, and $\langle111\rangle$, with the propagation vector directed along pseudocubic [111], i.e., monoclinic [101]. The moments on the two Fe sites were constrained to be equal and the Fe^{4+} form factor was assigned. Twelve atomic positional parameters, five isotropic temperature factors, ten profile parameters, a zero-point correction, and an overall scale factor were included in the refinement. The best fits were obtained with the helical axis directed along or fairly close to the monoclinic [101] axis, and gave a Fe moment of about $3.0\mu_B$. A slightly improved fit was obtained when the moments at the two Fe sites were refined independently, yielding values of 2.5 and 3.5 (or 3.5 and 2.5) μ_B, respectively, for Fe1 and Fe2. From the refinement alone it is not possible to distinguish between these two sets of values, but clearly only the first set are consistent with the bond valence calculation described above. The results of this refinement for the [101] spiral are summarized in Table VIII, model 1A, and the good quality of the fit is demonstrated by the low values of the goodness-of-fit residuals ($R_{\rm wp}$, $R_{\rm nuc}$, $R_{\rm mag}$, and χ^2). Additional refinements were carried out with the propagation vector directed along each of the other pseudocubic $\langle111\rangle$ directions. In each case the best fits were obtained with the spiral normal along or close to the direction chosen, and the refined values were essentially identical to those in Table VIII.

Although in general this simple model accounts quite well for the magnetic intensities, a closer examination of individual magnetic peak profiles reveals some significant discrepancies. This is illustrated in Fig. 11(a) for the second magnetic peak at $2\theta\sim27°$, which is a doublet composed of the $\pm(-\delta_m,0,2-\delta_m)$ and $\pm(1-\delta_m,\pm1,-\delta_m)$ satellites. Further refinements were carried out in which the propagation vector and the helical axis were no longer constrained to lie along the [101] direction, resulting in better goodness-of-fit residuals $R_{\rm mag}$ and χ^2 and a clearly-improved fit to the peak profile [Fig. 11(b)]. The resulting propagation vector deviates from the monoclinic [101] direction by about 1°, and the helical axis is now much closer to the monoclinic [112] direction, i.e., pseudocubic [101]. The results are listed in Table VIII, model 1B, and part of the profile fit and difference plot in Fig. 12.

The second model considered was a sinusoidal amplitude-modulated structure. An analogous set of refinements to

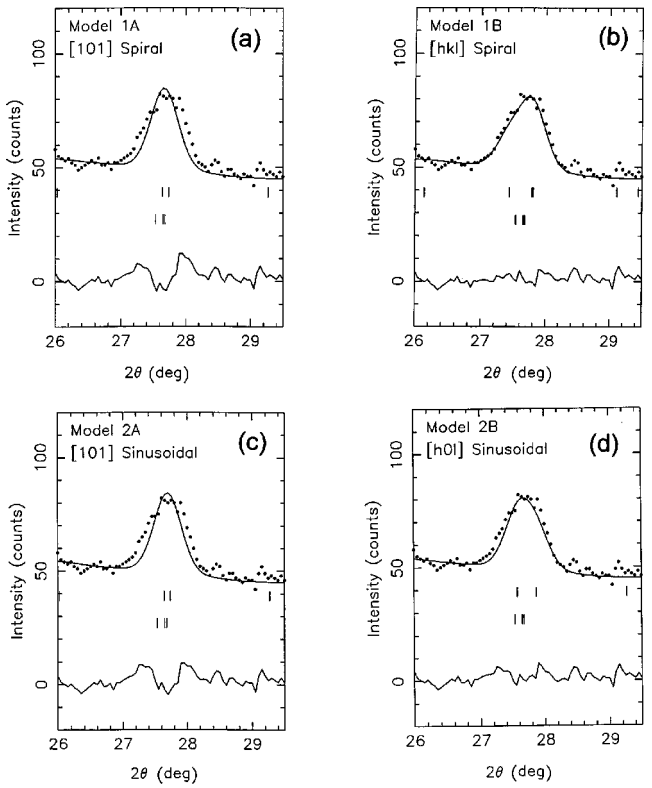

FIG. 11. Profile fits and difference plots for the second magnetic peak in the 15-K pattern for different magnetic models and propagation vectors as described in the text and Table VIII: (a) spiral with $\delta_a=\delta_c=\delta_m$, $\delta_b=0$; helical axis [101] (model 1 A) (b) spiral with $\delta_a\neq\delta_b\neq\delta_c$; helical axis [*hkl*] (model 1B) (c) sinusiodally modulated with $\delta_a=\delta_c=\delta_m$, $\delta_b=0$; moment direction [010] (model 2A) (d) sinusoidally modulated with $\delta_a\neq\delta_c$, $\delta_b=0$; moment direction $[0kl]$ (model 2B).

those described above was carried out with the magnetic moments directed along the principal pseudocubic directions ⟨100⟩, ⟨110⟩, and ⟨111⟩, and the propagation vector directed along monoclinic [101]. In this case the best fit was obtained

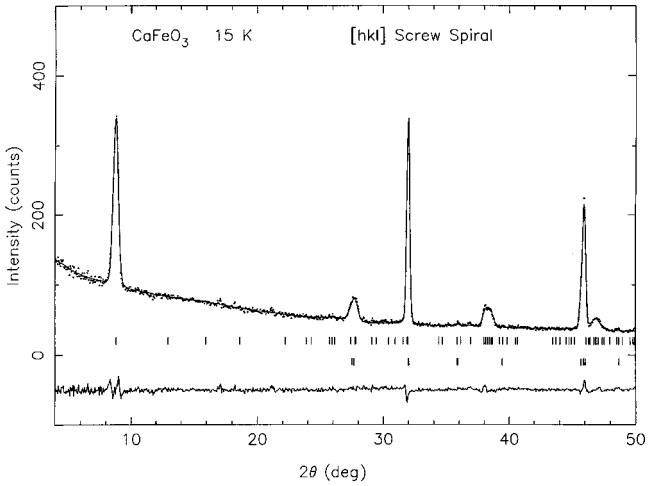

FIG. 12. Profile fit and difference plot for the low angle region of the neutron pattern for $CaFeO_3$ at 15 K for model 1B as described in text. The short vertical markers just below the profile plot indicate the calculated positions for magnetic and nuclear peaks (upper and lower rows, respectively).

with the direction of the moments along monoclinic [010], corresponding to pseudocubic $[1\bar{1}0]$, and yielded a maximum amplitude for the Fe moment of about $4.3\mu_B$. When the moments at the two Fe sites were refined independently, there was a very slight improvement in the fit, with values of 3.5 and 5.0 (or 5.0 and 3.5) μ_B for Fe1 and Fe2, respectively. The results of this refinement are summarized in Table VIII, model 2A, and it is clear from the similarity of the goodness-of-fit residuals (magnetic R factor $R_{\rm mag}$ and χ^2) that it is not possible to discriminate between the spiral and sinusoidal models. Once again, there were noticeable discrepancies in the individual peak profile fits [Fig. 11(c)], and a further refinement in which the propagation vector and magnetic moment direction were allowed to vary yielded better residuals (Table VIII, model 2B) and a distinctly-improved fit [Fig. 11(d)].

All of the above refinements yielded essentially the same values for the atomic coordinates, which were in reasonable agreement with the x-ray values in Table V, the average discrepancy being about 3σ. However, the mean bond lengths for Fe1-O and Fe2-O (1.91 and 1.93 Å) did not show clear evidence of charge order as in the x-ray refinement, which we believe is a consequence of the high degree of pseudosymmetry, the much lower resolution and peak-to-background discrimination of the neutron pattern, and the many overlapping magnetic peaks.

The results obtained for the simple screw spiral model with a single Fe moment are in good agreement with those reported by Kawasaki *et al.*[7] However, we find that improved fits are obtained when the propagation vector and helical axis are allowed to deviate from the pseudocubic [111] direction, and also when individual moments are assigned to the Fe1 and Fe2 atoms. Furthermore, we have extended the analysis to a sinusoidally modulated structure, and find that this model fits the data equally well. The two structures are illustrated schematically in Fig. 13. A screw spiral configuration has also been reported for $SrFeO_3$ by Takeda *et al.*,[6,14] and for $SrFeO_{2.9}$ by Oda and colleagues.[36,37] In light of the fact that the individual magnetic moments associated with the sinusoidal structure lie outside of the range of values that would be physically realistic for Fe^{3+} and Fe^{5+}, in the presence of significant covalency effects, a pure sinusoidal structure seems rather unlikely. However, we cannot rule out the possibility of some more complex intermediate type of fan structure. In view of these difficulties it is not possible to draw any firm conclusions about the electron configuration and the degree of covalency from the values of the magnetic moments. The simplest approximation would be to assume that the spiral model is correct, in which case the moments are significantly lower than the high-spin values of 3 and $5\mu_B$, and indicate a considerable degree of covalency.

It is interesting to note the similarity of the low-temperature neutron pattern for $CaFeO_3$ to that obtained by Battle *et al.*[38] for $Sr_{2/3}La_{1/3}FeO_{2.98}$, in which the Fe^{3+}:Fe^{5+} ratio is nearly 2:1. This compound has a hexagonally distorted perovskitelike structure, and the magnetic structure was described as a spin-density wave commensurate with a cell doubled along the pseudocubic [111] axis, corresponding to a modulation vector $[\delta,\delta,\delta]$ with $\delta=\frac{1}{6}$, in which adjacent layers of near-neighbor Fe^{3+} moments of $3.6\mu_B$ are coupled antiferromagnetically to each other, and ferromag-

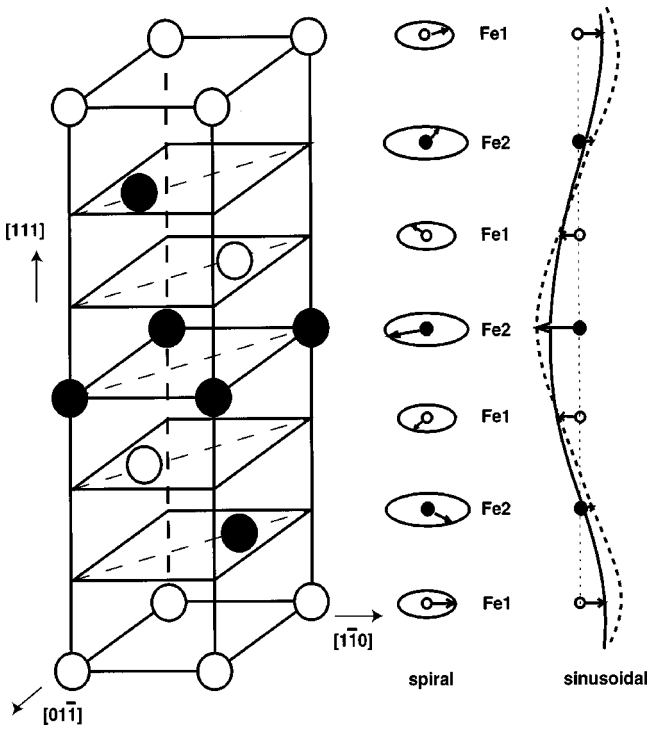

FIG. 13. Schematic illustration of the spiral and sinusoidal magnetic structures for $CaFeO_3$ at 15 K for the constrained models (Table VIII, models 1A and 2A).

netically to adjacent layers of near-neighbor Fe^{5+} moments of $2.7\mu_B$ on each side. However, these authors were unable to refine the long-range charge-ordered crystal structure, presumably because of the very high degree of pseudosymmetry. The magnetic structure is consistent with the predicted superexchange interactions,[39] and can be viewed as a square-wave amplitude-modulated structure locked into the lattice periodicity.

Clearly the situation is more complicated in $CaFeO_3$, where nearest-neighbor Fe^{3+} and Fe^{5+} ions would be expected to couple ferromagnetically, due to the superexchange interactions between half filled and empty e_g orbitals. The net result would be a simple ferromagnetic structure. For a ferromagnetic spiral to be stabilized, some kind of longer-range antiferromagnetic interaction is necessary. One possibility is the existence of significant superexchange interactions between next-nearest neighbors through two oxygen atoms. The Fe-O-O-Fe interactions involve the t_{2g} orbitals, which are half filled on both Fe^{3+} and Fe^{5+}, so that the next-nearest-neighbor interaction would be antiferromagnetic. Such behavior is known to occur in some ordered perovskite-type $A_2BB'O_6$ structures containing small B' ions.[40,41] For example, in Ba_2LaRuO_6 and Ba_2CaRuO_6, where the nearest neighbors are diamagnetic, the antiferromagnetic Ru^{5+}-O-O-Ru^{5+} coupling has been shown to be the dominant superexchange interaction.[42] In Ba_2CoReO_6, where both octahedral cations possess unpaired d electrons, these interactions lead to a modulation of a ferrimagnetic structure in which near-neighbor Co and Re moments are coupled antiparallel, with the propagation vector lying along a cubic $\langle 001 \rangle$ direction.[43] However, in each of the above examples the M-O-O-M coupling involved a $4d$ or $5d$ transition metal. The fact that $3d$ orbitals have a reduced spatial extent, with respect to the $4d$ and $5d$ orbitals, brings into question the importance of next-nearest-neighbor coupling in $CaFeO_3$. Another possible source of the antiferromagnetic interaction is the t_{2g}-Oπ-t_{2g} interactions between nearest neighbors, which is antiferromagnetic due to the fact that t_{2g} orbitals are half filled on both Fe^{3+} and Fe^{5+}. This type of coupling could also extend to next-nearest-neighbor (111) planes through Fe^{3+}-O π-Fe^{5+}-O π-Fe^{3+} linkages. This interaction is of course opposed by the ferromagnetic coupling of the e_g orbitals, but the competition between these two could lead to the observed canted structure.

CONCLUSIONS

Using powder-diffraction techniques, the room-temperature and low-temperature crystal structures of $CaFeO_3$ have been determined for the first time. At 300 K the crystal structure is distorted from the ideal cubic perovskite structure (adopted by $SrFeO_3$) by octahedral tilting. The octahedral tilting distortion in $CaFeO_3$ is identical to that seen in $GdFeO_3$ and $CaTiO_3$. Below T_{CD} ($\sim$290 K) two distinct types of Fe site develop, lowering the symmetry to monoclinic. In addition to the octahedral tilting distortion, the low-temperature structure exhibits rock-salt-type ordering of $Fe^{4+\delta}$ and $Fe^{4-\delta}$. Bond valences indicate that $\delta \cong 0.55$. Comparison of the 15- and 300-K crystal structures shows that the CD phase transition can be described as the condensation of a phonon breathing mode and the development of a charge-density wave. The temperature evolution of the unit-cell parameters indicate that the transition is second order. The low-temperature magnetic data can be fit equally well by a screw spiral structure similar to that reported by Kawasaki *et al.*[7] or by a sinusoidal amplitude-modulated structure. In both cases, the fit improves very slightly when the values of the moments at the two Fe sites are allowed to take different values; 2.5 and $3.5\mu_B$ for the spiral structure, and maximum amplitudes of 3.5 and $5.0\mu_B$ for the sinusoidal structure. Finally, we have shown that the CD induces only subtle changes in the x-ray-diffraction pattern and that very high quality diffraction data is absolutely necessary in order to detect it.

After preparation of this manuscript, but prior to submission, it came to our attention that a detailed neutron-diffraction study of $CaFeO_3$ was being carried out in Japan by T. Takeda *et al.*[44] Regarding the rock salt ordering of Fe^{3+}/Fe^{5+}, which drives the orthorhombic to monoclinic transition, their findings are in good agreement with ours.

ACKNOWLEDGMENTS

We thank M. Takano for providing the sample which provided the impetus for this work. We gratefully acknowledge several useful discussions with J. Rodriguez-Carvajal concerning the application of his FULLPROF program to incommensurate magnetic structures, and B. Toby for assistance with the neutron data collection at the BT1 neutron powder diffractometer, Center for Neutron Research, National Institute of Science and Technology. Work at Brookhaven was supported by the U.S. Department of Energy, Division of Materials Sciences, under Contract No. DE-AC02-98CH10886.

*Electronic address: woodward@chemistry.ohio-state.edu
†Present address: Institute for Materials Science, National Center for Scientific Research ''Demokritos,'' 15310 Agia Paraskevi Athens, Greece.

[1] E. O. Wollan and W. C. Koehler, Phys. Rev. **100**, 545 (1955).
[2] J. Rodriguez-Carvajal, M. Hennion, F. Moussa, and A. H. Moudden, Phys. Rev. B **57**, 3189 (1998).
[3] J. B. Goodenough and J.-S. Zhou, Chem. Mater. **10**, 2980 (1998).
[4] H. Watanabe, J. Phys. Soc. Jpn. **12**, 515 (1957).
[5] J. B. MacChesney, R. C. Sherwood, and J. F. Potter, J. Chem. Phys. **43**, 1907 (1965).
[6] T. Takeda, Y. Yamaguchi, and H. Watanabe, J. Phys. Soc. Jpn. **33**, 967 (1972).
[7] S. Kawasaki, M. Takano, R. Kanno, T. Takeda, and A. Fujimori, J. Phys. Soc. Jpn. **67**, 1529 (1998).
[8] M. Takano, N. Nakanishi, Y. Takeda, S. Naka, and T. Takada, Mater. Res. Bull. **12**, 923 (1977).
[9] M. Takano, N. Nakanishi, Y. Takeda, and S. Naka, J. Phys. (Paris), Colloq. **40**, C2-313 (1979).
[10] A. E. Bocquet, A. Fujimori, T. Mizokawa, T. Saitoh, H. Nagatame, S. Suga, N. Kimizuka, Y. Takeda, and M. Takano, Phys. Rev. B **45**, 1561 (1992).
[11] S. Licht, B. H. Wang, and S. Ghosh, Science **285**, 1039 (1999).
[12] For a discussion of the distinction between oxidation states and real charges, see A. W. Sleight, Proceedings of the Welch Foundation Conference on Chemical Research (1988), pp. 123–153.
[13] Y. Takeda, S. Naka, M. Takano, T. Shinjo, T. Takada, and M. Shimada, Mater. Res. Bull. **13**, 61 (1978).
[14] T. Takeda, S. Komura, and N. Watanabe, Proceedings of the Intenational Conference on Ferrites 3, Kyoto, Japan, edited by H. Watanabe, S. Iida, and M. Sugimoto (1980), pp. 385–8.
[15] F. Kanamaru, H. Miyamoto, Y. Mimura, M. Koizumi, M. Shimada, and S. Kume, Mater. Res. Bull. **5**, 257 (1970).
[16] S. Morimoto, T. Yamanaka, and M. Tanaka, Physica B **237–238**, 66 (1997).
[17] G. C. Smith, Synchrotron Radiat. News **4**, 24 (1991).
[18] A. C. Larson and R. B. Von Dreele, GSAS Software Suite, LANSCE-Los Alamos National Laboratory, Los Alamos, NM.
[19] J. Rodriguez-Carvaljal, Physica B **192**, 55 (1993).
[20] P. Suortti, J. Appl. Crystallogr. **5**, 325 (1972).
[21] P. G. Radaelli, D. E. Cox, M. Marezio, and S. W. Cheong, Phys. Rev. B **55**, 3015 (1997).
[22] P. M. Woodward, D. E. Cox, T. Vogt, C. N. R. Rao, and A. K. Cheetham, Chem. Mater. **11**, 3528 (1999).
[23] M. T. Anderson and K. R. Poeppelmeier, Chem. Mater. **3**, 476 (1991).
[24] A. M. Glazer, Acta Crystallogr., Sect. B: Struct. Crystallogr. Cryst. Chem. **B28**, 3385 (1972).
[25] P. M. Woodward, Acta Crystallogr., Sect. B: Struct. Sci. **B53**, 32 (1997).
[26] M. T. Anderson, K. B. Greenwood, G. A. Taylor, and K. R. Poeppelmeier, Prog. Solid State Chem. **22**, 197 (1993).
[27] The deviation of β from 90° may be rather small and often times can only be detected when the instrumental resolution, as well as the crystallite size and microstrain properties of the sample, result in sharp Bragg reflections. The absence of a detectable monoclinic distortion should never be taken as evidence for the lack of cation ordering.
[28] The CMPR software package was written by Brian Toby, Center for Neutron Research, NIST, Gaithersburg, MD, 20899.
[29] P. M. Woodward, J. Appl. Crystallogr. **30**, 206 (1997).
[30] K. Yvon, W. Jeitschko, and E. Parthe, J. Appl. Crystallogr. **10**, 73 (1977).
[31] H. Adachi and M. Takano, J. Solid State Chem. **93**, 556 (1991).
[32] J. A. Alonso, J. L. Garcia-Munoz, M. T. Fernandez-Diaz, M. A. G. Aranda, M. J. Martinez-Lope, and M. T. Casais, Phys. Rev. Lett. **82**, 3871 (1999).
[33] C. Chaillout, A. Santoro, J. P. Remeika, A. S. Cooper, G. P. Espinosa, and M. Marezio, Solid State Commun. **65**, 1363 (1988); D. E. Cox and A. W. Sleight, Acta Crystallogr., Sect. B: Struct. Crystallogr. Cryst. Chem. **B35**, 1 (1979).
[34] T. Shinjo, N. Hosoito, T. Takada, M. Takano, and Y. Takeda, Proceedings of the International Conference on Ferrites 3 (Ref. 14), pp. 393–396.
[35] A. Le Bail, H. Duroy, and J. L. Fourquet, Mater. Res. Bull. **23**, 447 (1988).
[36] H. Oda, Y. Yamaguchi, H. Takei, and H. Watanabe, J. Phys. Soc. Jpn. **42**, 101 (1977).
[37] H. Watanabe, H. Oda, E. Nakamura, Y. Yamaguchi, and H. Takei, Proceedings of the International Conference on Ferrites 3 Ref. 14, pp. 381–384.
[38] P. D. Battle, T. C. Gibb, and P. Lightfoot, J. Solid State Chem. **84**, 271 (1990).
[39] J. B. Goodenough, *Magnetism and the Chemical Bond* (Interscience, New York, 1963).
[40] S. Nomura and T. Nakagawa, J. Phys. Soc. Jpn. **21**, 1068 (1966).
[41] D. E. Cox, G. Shirane, and B. C. Frazer, J. Appl. Phys. **38**, 1459 (1967).
[42] P. D. Battle, J. B. Goodenough, and R. Price, J. Solid State Chem. **46**, 234 (1983).
[43] C. P. Khattak, D. E. Cox, and F. F. Y. Wang, in *Magnetism and Magnetic Materials—1972* edited by C. D. Grahan, Jr. and J. J. Rhyne AIP Conf. Proc. No. 10 (AIP, New York, 1973), pp. 674–8.
[44] T. Takeda, R. Kanno, Y. Kawamoto, M. Takano, K. Kawasaki, T. Kamiyama, and F. Izumi (unpublished).
[45] I. D. Brown, J. Appl. Crystallogr. **29**, 479 (1996).
[46] G. Thornton and A. J. Jacobson, Acta Crystallogr., Sect. B: Struct. Crystallogr. Cryst. Chem. **B34**, 351 (1978).
[47] T. Vogt, P. M. Woodward, P. Karen, B. A. Hunter, P. Henning, and A. R. Moodenbaugh, Phys. Rev. Lett. **84**, 2969 (2000).
[48] N. K. McGuire and M. O'Keeffe, Solid State Commun. **52**, 433 (1984).